The Interaction Investigation of LCN2 and DHODH Mediated Mitochondrial Ferroptosis in Sepsis-Induced Myocardial Injury

Lu Li , Yuping Li , Yixuan Hao , Mengjie Yu , Shicheng Xia , Jiahui Wang , Hongwei Ye , Qin Gao *

Posted Date: 3 June 2026

doi: 10.20944/preprints202606.0308.v1

Keywords: sepsis induce myocardial injury; mitochondrial derived ferroptosis; lipocalin-2; dihydroorotate dehydrogenase; STAT3

 doi:10.20944/preprints202606.0308.v1

Article

The Interaction Investigation of LCN2 and DHODH Mediated Mitochondrial Ferroptosis in Sepsis-Induced Myocardial Injury

Li Lu [1,2], Li Yuping [2,3], Hao Yixuan [1,2], Yu Mengjie [2,3], Xia Shicheng [4], Wang Jiahui [2], Ye Hongwei [1,2] and Gao Qin [1,2]*

[1] Department of Physiology
[2] Key Laboratory of Basic and Clinical Cardiovascular Diseases
[3] School of Life Sciences
[4] Department of Clinical Medicine, Bengbu Medical University, Bengbu 233000, China
* Correspondence: gaoqin@bbmu.edu.cn

Abstract

To investigate the role of knockdown of lipocalin-2 (LCN2) on DHODH mediated mitochondrial ferroptosis in sepsis-induced myocardial injury (SIMI) in mouse and cardiomyocyte injury model, and investigate the likely mechanism of STAT3. In this study, we established an sepsis induced cardiomyopathy (SIMI) model using cecal ligation and puncture (CLP) in mice. Mouse cardiac samples were used to identify the association between the serum lipocalin 2 (LCN2) level and spesis progression. Chemical inhibition of ferroptosis were conducted to illustrate the effect of ferroptosis upon SIMI.Then, mouse models with knockdown of LCN2 were used to ascertain the role of LCN2 upon ferroptosis and spesis. To interaction mechanism between LCN2 and DHODH was investigated. we overexpressed DHODH in mouse HL-1 cardiomyocytes using lentivirus, and established a lipopolysaccharide (LPS)-induced cardiomyocyte injury model. The results showed that in septic mice, the increase of LCN2 was correlated positively with myocardial severity, glutathione peroxidase 4 (GPX4) and dihydroorotate dehydrogenase (DHODH) mediated ferroptosis both occurred in SIMI. Inhibiting ferroptosis reduced LCN2 expression, thereby alleviated SIMI. Molecular docking and immunoprecipitation revealed strong binding between LCN2 and DHODH. Knockdown of LCN2 inhibited DHODH mediated ferroptosis, decreased phosphorylated STAT3 (p-STAT3) protein expression level, improved mitochondrial function, and mitigated SIMI. Meanwhile, exogenous recombinant LCN2 protein induced mouse cardiomyocyte ferroptosis. Overexpression of DHODH protected against LPS-induced cardiomyocyte injury. Inhibition of DHODH abolished knockdown-LCN2 induced decrease of p-STAT3 protein expression. However, after inhibition of mitochondrial GPX4 expression by Fin56, p-STAT3 protein was not changed. In summary, our study confirmed knockdown of LCN2 inhibited DHODH mediated ferroptosis in SIMI, inhibiting DHODH attenuated the protection of knockdown-LCN2 through inhibiting STAT3 phosphorylation. It provides the new insight for preventing sepsis-induced myocardial injury.

Keywords: sepsis induce myocardial injury; mitochondrial derived ferroptosis; lipocalin-2; dihydroorotate dehydrogenase; STAT3

1. Introduction

Sepsis induces multiple organ dysfunction syndrome (MODS) due to a dysregulated inflammatory response to infection, characterized by concurrent hyperinflammation and immunosuppression, with high morbidity and mortality rates globally [1]. One of the most severe complications of sepsis is myocardial injury, which often leads to sepsis induced cardiomyopathy (SIMI), manifesting as cardiac arrhythmias, heart failure, hypotension and myocardial inflammation,

 doi:10.20944/preprints202606.0308.v1

it significantly affects the prognosis of septic patients [2]. Recent studies have shown that cardiac dysfunction induced by sepsis is a major cause of sepsis-related mortality, accounting for 70-90% of cases [3].

The increasing evidences suggest that ferroptosis exacerbates sepsis-induced organ damage, leading to multiple organ dysfunction. Ferroptosis as a form of non-apoptotic cell death induced by ferrous ions (Fe^{2+}) has been widely recognized. Its primary mechanism involves cellular metabolic and redox imbalances, leading to the accumulation of iron-dependent phospholipid hydroperoxides (PLOOHs) and increasing lipid reactive oxygen species (ROS), which causes rapid, irreversible cellular damage. The morphological features include mitochondrial shrinkage, increased membrane density, and reduction or disappearance of mitochondrial cristae [4]. Mitochondrion as the most sensitive organelle to cellular damage or injury, plays the central role in iron metabolism and energy metabolism, and it is a major source of intracellular ROS, thus closely associated with ferroptosis [5]. Recent studies indicate that ferroptosis is a key therapeutic target for cardiac diseases. Wang and Feng et al. found that the ferroptosis inhibitor ferrostatin-1 (Fer-1) effectively rescued doxorubicin-induced cardiac injury characterized by significant mitochondrial morphological and functional changes in mice [6,7]. Sofia et al showed that inhibiting cardiac glutathione metabolism, resulting in decreased glutathione peroxidase levels, increased cardiac lipid peroxidation, leading to ferroptosis and exacerbating mitochondrial cardiomyopathy [8]. Liu et al. discovered that melanin nanoparticles could inhibit intracellular iron accumulation, improve mitochondrial function, suppress ferroptosis, and ameliorate sepsis-induced myocardial injury [9]. Therefore, targeting mitochondrial derived ferroptosis may be a crucial strategy for protecting cardiac function, with significant research and translational potential in SIMI. DHODH as the rate-limiting enzyme for de novo pyrimidine nucleotide synthesis in mitochondria links de novo pyrimidine nucleotide biosynthesis with the electron transport chain (ETC) on complex III through coenzyme Q [10]. DHODH is also an essential enzyme for synthesizing new pyrimidines and a therapeutic target for various cancers such as melanoma, acute myeloid leukemia, glioblastoma, lung cancer, pancreatic cancer, and prostate cancer [11–16]. Recent studies suggest that DHODH inhibition may reduce tumor growth in vivo by reducing the occurrence of ferroptosis [10], however, its role in SIMI remains unknown. Therefore, in this study, we focus on mitochondrial DHODH mediated ferroptosis in SIMI.

Lipocalin-2 (LCN2) is a 23 kDa antimicrobial polypeptide that was initially discovered in the secondary granules of human neutrophils, playing a role in innate immunity by sequestering iron to limit bacterial growth. LCN2 is expressed in various normal tissues, including thymus, kidneys, bone marrow and adipose tissue, but its expression is low or absent in normal brain, heart, colon and skeletal muscle. However, inflammation and metabolic diseases induced LCN2 high-expression [17–20]. Vazquez et al. found that LCN2 expression was strongly induced in liver and lung of CLP-induced sepsis animal models [21]. Currently, LCN2 is known to participate in the regulation of inflammatory responses in the cardiovascular system by modulating the expression and secretion of inflammatory mediators such as pro-inflammatory cytokines and cell adhesion molecules, leading to endothelial inflammation and vascular injury. Studies have shown a positive correlation between LCN2 expression levels and heart failure [22]. LCN2 is upregulated during myocardial ischemia-reperfusion, coronary artery disease, and myocardial infarction [23–25]. Additionally, hypoxia induces LCN2 mRNA and protein expression in HL-1 cells [26]. Aigner et al observed the elevated LCN2 levels after heart transplantation in rodents [24]. These findings suggest that LCN2 can be a biomarker for the severity and high mortality of heart disease.

As a transporter which regulates intracellular and extracellular iron levels, LCN2 directly controls iron metabolism. Bacterial growth and metabolism require iron, invading pathogens utilize iron-binding proteins to acquire iron from the host's transferrin and lactoferrin [27,28]. Research indicates that LCN2 promotes lipid peroxidation accumulation by increasing intracellular Fe^{2+}, thereby exacerbating ferroptosis [29]. Our previous studies showed myocardial LCN2 level was increased, which closely associated with ferroptosis and iron metabolism in CLP mouse model

 doi:10.20944/preprints202606.0308.v1

[30,31]. Therefore, we would like to explore the intensive mechanism of LCN2 in septic mitochondrial ferroptosis.

Signal transducer and activator of transcription 3 (STAT3) can regulate the biological behaviors of cells by mediating extracellular signals of inflammatory mediators. It is an indispensable key molecule in the process of inflammation formation. When cells are subjected to relevant stimuli, such as inflammation, hypoxia, and ischemia, STAT3 in the cytoplasm undergoes phosphorylation and translocates to the nucleus to exert transcriptional regulatory functions [32,33]. Studies have shown that the upregulation of STAT3 signaling pathway can promote ferroptosis [34]. LCN2 has been identified as a pro-inflammatory factor to induce STAT3 expression [35]. Jiang discovered that target LCN2 can effectively inhibit inflammation, improve mitochondrial dysfunction, inhibit cardiomyocyte ferroptosis, and alleviate SCM [36], but the mechanism is not indicated. In our study, we want to intensively observe the relationship of p-STAT3, LCN2 and ferroptosis in SIMI [36]. Therefore, firstly, we explored whether LCN2 induced mitochondrial ferroptosis in SIMI through knockdown of LCN2 in mice model, and analyze the change of mitochondrial ferroptosis through inhibiting DHODH and mitochondrial GPX4, furtherly used DHODH overexpression and exogenous rLCN2 in cardiomyocyte model to intensively explore the interaction of LCN2 and DHODH. This study aims to seek for the new potential therapeutic strategy for sepsis.

2. Materials and Methods

2.1. Experimental Animals

All specific pathogen-free (SPF) grade healthy C57BL/6 mice (male, 6-8 weeks old, weighing 18-22 g) were purchased from Jiangsu Qinglongshan Biological Technology Co., Ltd., production license number SCXK (Su) 2024-0001. The animals were housed in an SPF-grade animal facility, maintained on a 12-hour dark/light cycle, with ad libitum access to food and water. The temperature was maintained at 22-25 °C, and the humidity was kept at 60 %-70 %. This study was approved by the Ethics Committee of Bengbu Medical College (Ethics number: [2023] No. 520), and all experiments complied with the “Regulations on the Administration of Laboratory Animals.”

2.2. Cecal Ligation and Puncture (CLP) Mouse Model

CLP is used in rodents for mimic the clinical course of sepsis [37]. The mice were anesthetized using a mixture of 3% isoflurane. After shaving and disinfecting the abdominal area, a midline incision was made with ophthalmic scissors. The cecum was ligated at the distal third with a 3-0 non-absorbable surgical suture and punctured twice at the distal end with an 18 G needle, gently squeezing out a small amount of feces. The cecum was then returned to the abdominal cavity and the incision was closed. In the sham operation group, the cecum was only exposed without ligation and puncture. Postoperatively, the mice were placed in a prone position and injected subcutaneously with pre-warmed 37°C saline (10 ml/kg; s.c.) for fluid resuscitation. Before echocardiography, the severity of sepsis was assessed using Mouse Sepsis Score (MSS). The MSS method calls for 7 observations: physical characteristics, degree of awareness, activity, reaction to stimulation, eyes, respiratory rate, and respiratory quality. The average of these seven elements yields the standard MSS score [38]. After echocardiography, the mice were deeply sedated for blood collection via retro-orbital bleeding. Following blood collection, the hearts were collected and stored at -80°C for further analysis.

2.3. Construction of shRNA and Lentiviral Vectors

Genechem Co., Ltd. (Shanghai, China) constructed short hairpin RNA (shRNA) targeting mouse Lipocalin-2 (LCN2) was used to interfere with LCN2 expression, the shRNA sequence for LCN2 is as follows: target sequence: 5′-GCTTTACGATGTACAGCACCA-3′. LCN2 or AAV9-EGFP-NC was injected into the mice tail vein for 3 weeks to downexpress LCN2 before CLP.

 doi:10.20944/preprints202606.0308.v1

The lentivirus for overexpressing dihydroorotate dehydrogenase (DHODH) to generate the stable overexpression cells. The mouse HL-1 cardiomyocytes were transfected by DHODH-EGFP or NC-EGFP. The positive transfected cells were selected with puromycin at 2.5 μg/mL for 2 weeks post-transfection. The efficiency of infection and transfection was confirmed by Western blot and quantitative real-time PCR (qRT-PCR).

2.4. Quantification of Cardiac Injury and Functional Assessment In vivo

The echocardiography was performed in vivo within 24 h post-CLP using Vevo-2100 imaging system (FujiFilm VisualSonics, Canada). The cardiac function was assessed by measuring the left ventricular ejection fraction (EF%), fractional shortening (FS%) and cardiac output (CO).

For evaluation of cardiac injury in mice [39,40], creatine kinase-MB (CK-MB) and lactate dehydrogenase (LDH) levels in serum were measured using the related assay kits (E006-1-1, Nanjing Jiancheng Bioengineering Institute and BC0685, Solarbio, China respectively)

2.5. Determination of MDA and SOD Levels

According to the manufacturer's instructions, malondialdehyde (MDA) and superoxide dismutase (SOD) levels in cardiac tissue were measured using the related commercial assay kit (A003-1 and A001-3, Nanjing Jiancheng Bioengineering Institute, China).

2.6. Enzyme-Linked Immunosorbent Assay (ELISA) Analysis

According to the manufacturer's protocols, the levels of serum inflammatory cytokines IL-6 and TNF-α, as well as the levels of myocardial LCN2 and DHODH, were measured and quantified using ELISA kits. The specific kits were obtained from Jiangsu Jingmei BioTech Co., Ltd: mouse IL-6 (JM-02446M1), TNF-α (JM-02415M1), LCN2 (JM-12543M1), and DHODH (JM-12822M).

2.7. Hematoxylin and eosin (H&E) staining Observation

For histological analysis, the harvested heart tissues were fixed in 4% paraformaldehyde for 72 h, dehydrated, cleared, paraffin-embedded, and sliced into 6-μm-thick sections for hematoxylin and eosin (H&E) staining. The morphological changes in cardiac tissues, such as inflammatory infiltration and fibrotic areas, were evaluated under an optical microscope (NIKON ECLIPSE E100, Japan) to assess pathological conditions.

2.8. Transmission Electron Microscopy (TEM) Observation

The myocardial tissue (≤ 1 mm^3) was rapidly excised from the left ventricle and washed with pre-cooled PBS. Subsequently, the tissues were immediately fixed overnight at 4 °C in a 2.5% glutaraldehyde solution buffered with phosphate (pH 7.4). After being embedded, the samples were sliced into ultrathin Sects. (50 nm) and stained with uranyl acetate and lead citrate before being observed using an electron microscope (HITACHI, HT7800, Japan).

2.9. Detection of ROS Levels in Myocardial Tissue using DHE Fluorescent Probe

The myocardial tissue was washed with PBS (pH 7.4) and placed in embedding molds. Embedding medium was immediately added, and the samples were frozen for sectioning. The tissue was sectioned into 6 μm thick slices using a cryostat and mounted on adhesion slides. The sections were incubated in a working solution of 10 μmol/L dihydroethidium (DHE) in a water bath at 37°C for 30 min in dark. Following incubation, the nuclei were counterstained with 5 μg/ml DAPI working solution. The changes in fluorescence intensity were observed using an inverted fluorescence microscope (Zeiss, Obsever Z1, Germany).

 doi:10.20944/preprints202606.0308.v1

2.10. RNA Extraction using TRIzol and Quantitative Real-Time Polymerase Chain Reaction (qPCR)

Total RNA was extracted from heart tissue and cultured HL-1 cells using TRIzol reagent (15596026, Invitrogen, USA). The RNA was then reverse transcribed into cDNA using the FastKing cDNA First Strand Synthesis Kit (KR118, Tiangen Biotech, China). qPCR was performed using the SuperReal PreMix Plus (FP205, Tiangen Biotech, China). Gene expression levels were normalized to GAPDH levels to determine relative expression levels, and fold changes were calculated using the 2-ΔΔCT method. The following primers were used:

Objective gene	Primer sequences	product length（bp）
LCN2	F:5′ TGGCCCTGAGTGTCATGTG 3′ R:5′ CTCTTGTAGCTCATAGATGGTGC 3′	239
DHODH	F:5′TCTTCACCTCTTACCTGACAGC 3′ R:5′CATGTTGGAGTCCTGAAACGTA3′	164
GAPDH	F:5′ GACATGCCGCCTGGAGAAAC 3′ R:5′ AGCCCAGGATGCCCTTTAGT 3′	92

2.11. Molecular Docking Analysis and Co-Immunoprecipitation (Co-IP) to Observe the Relationship Between LCN2 and Ferroptosis-Related Proteins

For predicting the direct binding models of LCN2 protein with GPX4, FSP1, and DHODH, we first retrieved the detailed information including structural files and sequence data from the Uniprot database for LCN2, GPX4, and DHODH. The PDB IDs were as follows: LCN2: 3T1D, GPX4: 6hkq, DHODH: 7Z6C. We used AlphaFold 2 protein structure prediction tool to predict the full-length structure of FSP1.

The protein structures were processed using UCSF Chimera 1.17.1 software by adding hydrogens, calculating and adding charges, and performing energy minimization. Molecular docking experiments between these proteins were conducted using ClusPro software. After docking, the structures with the best binding energies to LCN2 were visualized and processed using Maestro 13.5 software.

For Co-IP experiments, Protein A+G magnetic beads (P2108-5, Beyotime, China) were added to EP tubes containing IP and IgG groups. The beads were washed with PBS by inverting and then placed on a magnetic stand to remove the supernatant, repeated twice. LCN2 antibody was added to the IP group tubes according to the manufacturer's instructions, while an equal amount of IgG antibody (A7007, Beyotime, China) was added to the control group tubes. The tubes were incubated on a shaker at 4 °C for 12 h. After incubation, the magnetic beads were washed 3 times, and then the total protein from the CLP group was added to each tube and incubated on a shaker at 4 °C for 12 h. Input positive control, IP group, and IgG negative control samples were boiled in 3× sample buffer at 95 °C for 5 min and cooled to 4 °C before western blot analysis to detect the co-expressions of LCN2 with GPX4, DHODH and FSP1.

2.12. Mouse HL-1 Cell Culture

The mouse HL-1 cells were cultured in Claycomb Medium (iCell-0012, Shanghai iCell) supplemented with 10% FBS at 37°C in a humidified atmosphere containing 5% CO_2 using a CO_2 incubator (HF100, Thermo Fisher Scientific, USA). To verify ferroptosis induced by LPS, the HL-1 cells were treated with 20 μg/ml LPS (L3024, Sigma-Aldrich, USA) for 48 h after determining the appropriate concentration through viability analysis [31]. Except control group, as a positive

 doi:10.20944/preprints202606.0308.v1

ferroptosis group, the cells were treated with 10 μM RSL3 (SML2234, Sigma-Aldrich, USA) for 24 h. To investigate the relationship between LCN2 and ferroptosis, the cells were treated with 1 μg/ml recombinant LCN2 protein (rLCN2) (CM17, Novoprotein, China) for 24 h [41],. To further investigate the relationship between LCN2 and DHODH in sepsis, the HL-1 cells with overexpressing-DHODH were treated with 1 μg/ml rLCN2 and LPS for 24 h.

2.13. Analysis of Cell Viability and LDH Levels

The cell viability was assessed using the Cell Counting Kit-8 (CCK-8) (BS350A, Biosharp, China) after different treatments. The HL-1 cells were seeded into 96-well plates and incubated with CCK-8 working solution (100 μl/well in medium) at 37 °C in a CO_2 incubator for 1 h. The absorbance was measured at 450 nm using a microplate reader (Bio-Tek, USA).

2.14. Cell ROS Measurement by DHE

The cells were washed twice with warm PBS. Following the manufacturer's instructions, a working solution of 10 μM DHE probe (S0063, Beyotime, China) diluted in MEM medium was added. The cells were then incubated in a 5% CO_2 incubator at 37°C for 30 min in the dark. Subsequently, cells were fixed with 4% paraformaldehyde at room temperature for 20 min. After permeabilization with permeabilization buffer at room temperature for 10 min, cells were incubated with 5 μg/ml DAPI working solution (S0063, Beyotime, China) at 37 °C for 7 min in the dark to counterstain the nuclei. Images were captured using a Zeiss inverted fluorescence microscope (Zeiss, Obsever Z1, Germany).

2.15. Mitochondrial ROS Measurement by MitoSOX

The cells were washed twice with warm Hank's Balanced Salt Solution (HBSS) (BL561A, Biosharp, China). A working solution of 5 μmol/ml MitoSOX fluorescent probe (M36008, Thermo Fisher Scientific, USA) prepared in 1 ml MEM medium was added to the cells, incubated at 37 °C for 30 min. Then, the cells were washed 3 times with PBS according to the manufacturer's instructions. Subsequently, cells were fixed with pre-warmed 4% paraformaldehyde at room temperature for 20 min. After permeabilization with permeabilization buffer (P0097, Beyotime, China) at room temperature for 10 min, the cells were counterstained with 5 μg/ml DAPI working solution to stain the nuclei. The detection of mitochondrial ROS were performed using a two-photon laser scanning confocal microscope (FV-1200MPE-SHARE, Olympus, Japan). FlowJo and GraphPad Prism 9 software was used to analyze the results.

2.16. Mitochondrial Imaging and Fe^{2+} Content Measurement

To confirm the mitochondrial damage caused by LPS, RSL3 and rLCN2, and the protective effect of DHODH, mitochondria were stained, and mitochondrial membrane potential (MMP) were evaluated. The cells were washed twice with warm HBSS. According to the manufacturer's instructions, 1 ml MEM medium containing 0.1 μmol/L MitoBright LT Deep Red fluorescent probe (MT12, Japan Dojindo) was added, and the cells were incubated in a light-protected incubator at 37 °C for 15 min. After incubation, cells were washed 3 times with pre-warmed HBSS. Then, the cells were treated with HBSS containing 1 μmol/L Fe^{2+} (F374, Japan Dojindo) and incubated at 37 °C in a 5% CO_2 incubator for 30 min. The detection of MMP and Fe2+ Content were performed using a two-photon laser confocal microscope (FV-1200MPE-SHARE, Japan Olympus). The results were analyzed by FlowJo and GraphPad Prism 9 software.

2.17. Immunofluorescence (IF)

The Cells were washed 3 times using PBS, fixed with 4% paraformaldehyde（BL539A, China Biosharp）at room temperature for 20 min. Immunostaining permeabilization buffer was applied for 10 min, followed by blocking with 5% bovine serum albumin (BSA, 143183, Germany Biofroxx) at 37 °C for 90 min. The cells were then incubated overnight at 4°C with rabbit anti-LCN2 antibody (26991-

 doi:10.20944/preprints202606.0308.v1

1-AP, China Proteintech), DHODH antibody (14877-1-AP, China Proteintech), STAT3 antibody (AF6294, USA Affinity), and p-STAT3 antibody (AF3293, USA Affinity). After washing 3 times with PBS, cells were incubated with corresponding goat anti-rabbit IgG-Alexa Fluor secondary antibody (ZF-0516, Beijing Zhongsheng Golden Bridge Biotechnology Co., Ltd.) diluted 1:200 at 37°C for 30 min. DAPI staining (C1002, Beyotime, China) was performed for 7 min. Images were acquired using a Zeiss fluorescence inverted microscope (Zeiss, Observer Z1, Germany).

2.18. Western Blotting

Mitochondria were isolated from fresh heart tissue using the Tissue Mitochondria Isolation Kit (C3606, Beyotime, China) as per the manufacturer's instructions. Cytoplasmic proteins were also extracted. The heart tissue and HL-1 cell proteins were extracted using RIPA lysis buffer (P0013B, Beyotime, China) supplemented with protease and phosphatase inhibitors, and lysed on ice for 30 min. The lysates were then centrifuged at 4 °C for 15 min. Protein concentration was determined using the BCA protein assay. Protein samples (20 μg per lane) were separated on 10% SDS-PAGE gels and subsequently transferred onto PVDF membranes (IPVH0001, Merck Millipore, USA). PVDF membranes were blocked with non-protein blocking buffer (PS108, Shanghai Yenzyme Biotech, China) at room temperature for 30 min. Membranes were incubated overnight at 4 °C with the following primary antibodies: GAPDH (1:7000, abs132004, Absin, China), LCN2 (1:1000, AF1857, R&D Systems, USA), GPX4 (1:3000, ab125066, Abcam, USA), xCT (1:5000, ab175186, Abcam, USA), Ferritin (1:1000, ab75973, Abcam, USA), FPN1 (1:2000, NBP1-21502, NOVUS, USA), COX IV (1:2000, WL02203, Wanlei Bio, China), Cytochrome C (1:2000, WL02410, Wanlei Bio, China), STAT3 (1:1000, AF6294, Affinity, USA), Phospho-STAT3-Tyr705 (1:1000, AF3293, Affinity, USA). After washing with TBST (Tris-buffered saline with Tween-20) 3 times for 5 min each, membranes were incubated with appropriate horseradish peroxidase-conjugated secondary antibodies (1:5000, Affinity, USA) for 30 min at 4°C. Protein bands were visualized using a highly sensitive ECL (enhanced chemiluminescence) substrate (P90720, Millipore, USA). Band intensities were quantified using ImageJ software, and protein expression levels were normalized to GAPDH levels.

2.19. Statistical Analysis

The results are presented as the mean ± SD from at least three in dependent experiments using GraphPad Prism 9 (GraphPad Software, La Jolla, CA, USA). The significance of differences in the means of corresponding values among groups was determined by using one-way ANOVA followed by Tukey post hoc tests. Statistical significance was considered at $P < 0.05$.

3. Results

3.1. Sepsis Induced the Increase of Myocardial LCN2 Expression, and LCN2 Level is Positively Correlated with the Severity of Sepsis

We established the mouse sepsis model of by CLP operation, and the severity of sepsis was evaluated using MSS at 12h, 24h, 36h, 48h, and 72h post-surgery [38]. In the Figure 1A and Figure 1B, it was found that the myocardial injury was more severe in 12h and 24h after CLP, and LDH in CLP group was higher than in Sham group at other time periods (Figure 1D, $P<0.05$), indicating that sepsis model was successful. The cardiac function, CO, LVFS% and LVEF% in CLP12h and CLP24h groups were significantly decreased when compared with the Sham group ($P < 0.001$). In CLP36h, CLP48h and CLP72h groups, there was a gradual decline in CO, LVFS%, and LVEF% (Figure 1F-1H, $P < 0.01$). Additionally, CK level was increased obviously in CLP24h (Figure 1D, $P < 0.01$). Compared with the Sham group, LCN2 protein expression level in CLP12h and CLP24h groups was elevated (Figure 1G, $P < 0.01$).

In HL-1 cardiomyocyte injury model, when the cells were induced with LPS and RSL3 respectively, ROS levels in cells and mitochondria were both increased (Figure 1L, N, $P < 0.01$),

 doi:10.20944/preprints202606.0308.v1

intracellular Fe^{2+} level was elevated, and MMP was decreased significantly (Figure 1R). LCN2 protein level was increased (Figure 1P, T, $P < 0.01$), while the ferroptosis-related proteins GPX4 and DHODH were decreased (Figure 1Q, U, V, $P < 0.01$).

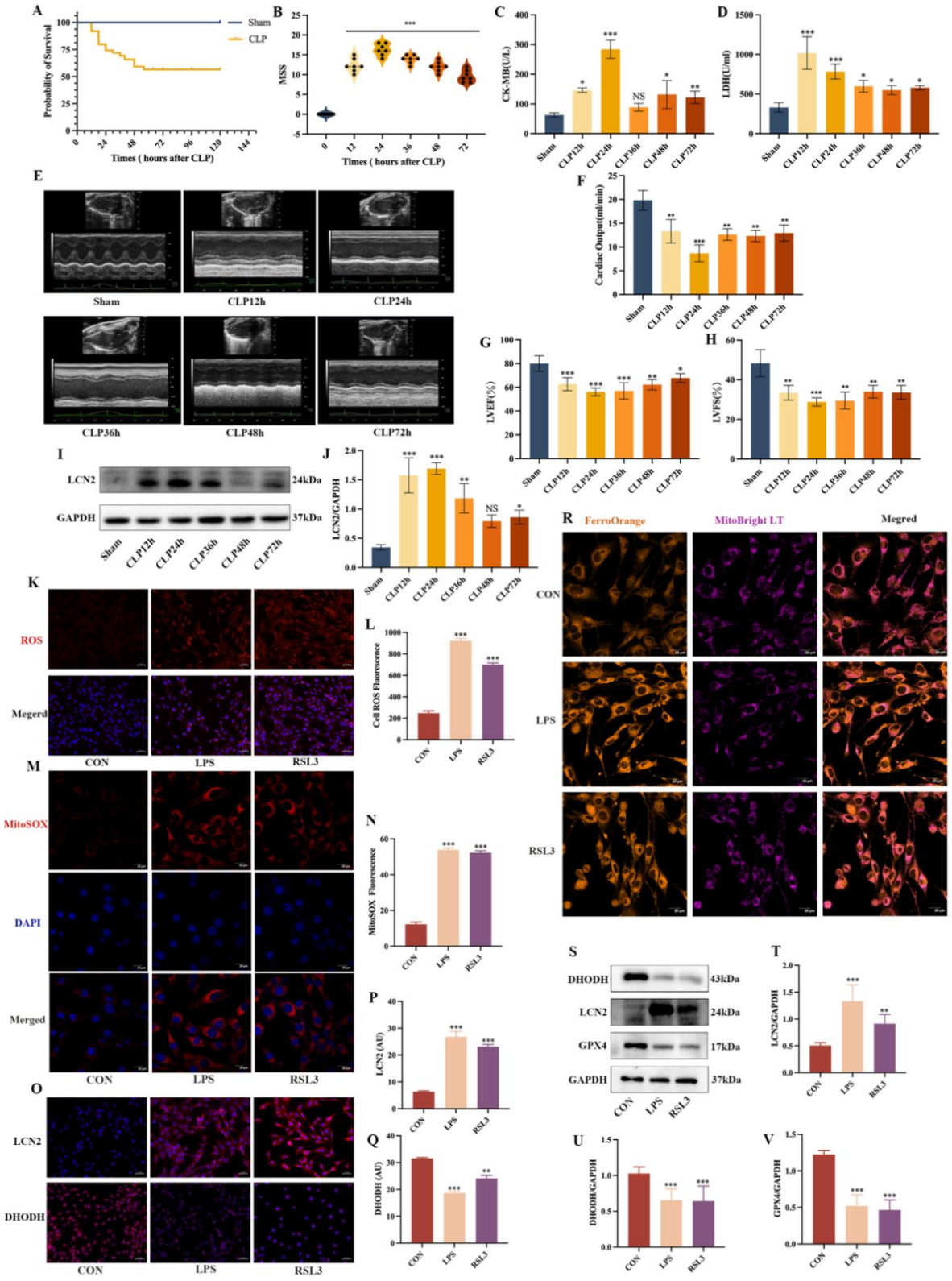

Figure 1. Elevated LCN2 level was associated with ferroptosis. A: Survival curves of cecal ligation and puncture B: Murine sepsis score (MSS). C-D: Serum CK-MB and LDH levels in each group. E: Evaluation of cardiac function by echocardiography. Representative M-mode images are shown (E). F-H: Echocardiographic parameters. cardiac output (F); left ventricle ejection fraction (G); left ventricular fractional shortening (H). I, S:

 doi:10.20944/preprints202606.0308.v1

Representative images of the Western blot results. Changes in the protein expressions of LCN2 (J, T) (n = 3-6), GPX4 (V) and DHODH (U) (n = 6). K: Representative images of fluorescence probe for ROS in HL-1 cardiomyocytes (n=6, scale bar= 50 μm). L: The ROS fluorescence in each group. M: Images of mitochondrial ROS in different groups. N: Mitochondrial ROS fluorescence intensity analysis. (n=5, scale bar= 20 μm). O: Images of LCN2 and DHODH (red) and DAPI (blue) immunofluorescence staining. P, Q: LCN2 and DHODH fluorescence intensity analysis. (n=6, scale bar= 50 μ m). R: Detection of intracellular $Fe^{2+}$and mitochondrial morphology of HL-1 cardiomyocytes in different groups (scale bar= 20 μm). Data are presented as mean ± SD. *****P < 0.0**01, **P < 0.01, *P < 0.05 vs Sham group, NS:P > 0.05 vs Sham group. ***P< 0.001, **P< 0.01 vs CON group.

3.2. Different Pathways of Ferroptosis were Happened in Sepsis-Induced Cardiac Injury

According to the above experimental results, further experiments were conducted at 24h post-CLP to investigate the different pathways of ferroptosis in septic conditions. In cardiomyocyte model, we further used ferroptosis chelating agent DXZ and ferroptosis inhibitor Fer-1 to observe the change of ferroptosis. The experimental design is shown in the Figure 2A. According to the results of myocardial ferroptosis related key proteins expressions---- total GPX4, total xCT, cytoplasm GPX4 (Cyto GPX4), ferroptosis suppressor protein 1 (Cyto FSP1), xCT (Cyto xCT), mitochondrial derived GPX4 (Mito GPX4), DHODH (Mito DHODH) and xCT (Mito xCT), the results showed that the different pathways of ferroptosis were occurred in CLP group (Figure 2 D-M, P < 0.01-0.001). Ferroptosis chelator DXZ and inhibitor Fer-1 both improved MSS scores (Figure 2B, P < 0.01) and decreased LCN2 protein expression in CLP mice (Figure 2C, P < 0.01).

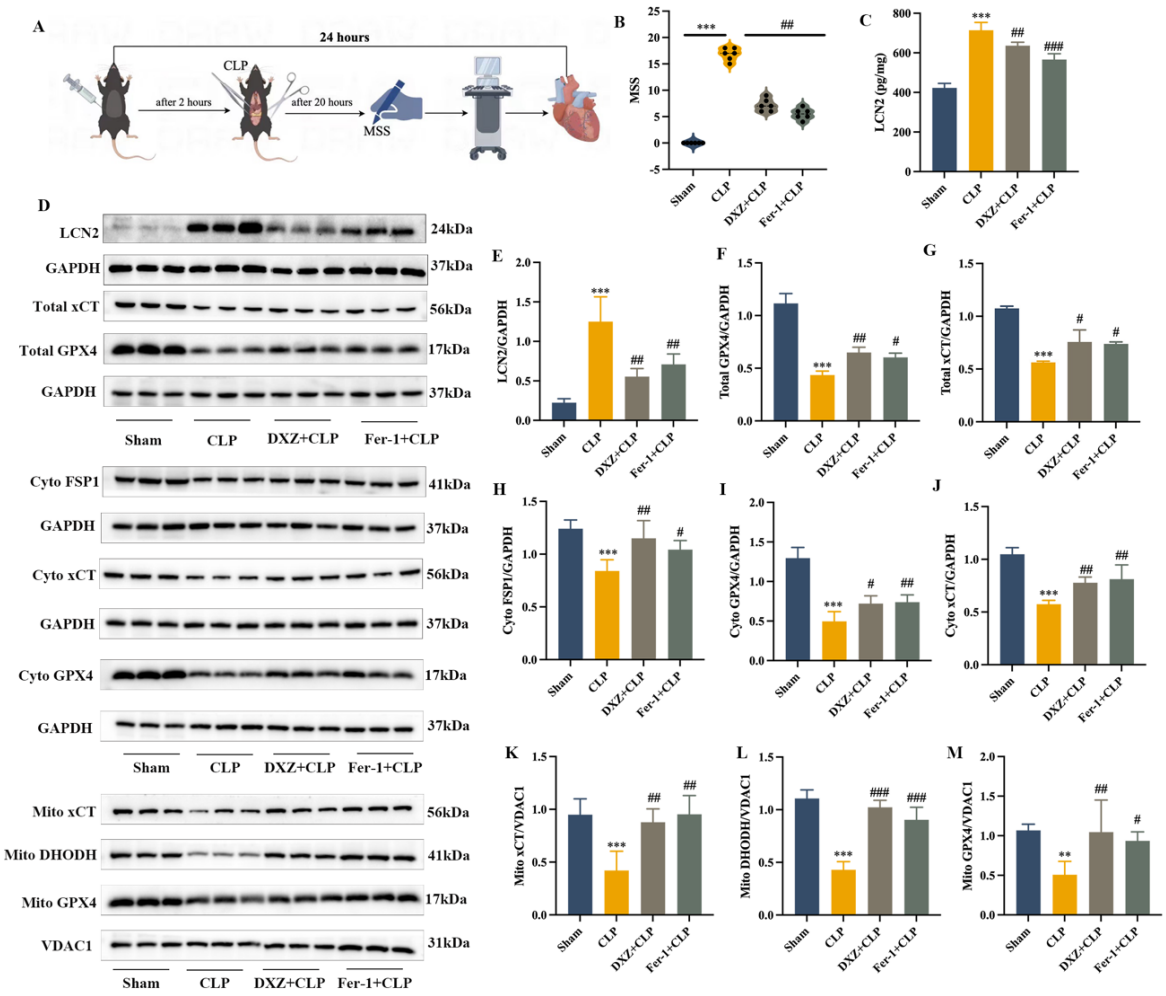

Figure 2. Different pathways of ferroptosis in sepsis-induced cardiac injury. A: Experimental design drawing. B: Murine sepsis score (MSS). C: The myocardial LCN2 level in each group. D: Representative images of the western

 doi:10.20944/preprints202606.0308.v1

blot results. Changes in the protein expressions of LCN2 (E), Total GPX4 (F), Total xCT (G) (n =3), Cyto FSP1 (H), Cyto xCT (I), Cyto GPX4 (J), Mito xCT (K), Mito DHODH (L) and Mito GPX4 (M) (n=6). $^{***}P < 0.001$ vs Sham group, $^{###}P< 0.001$, $^{##}P< 0.01$, $^{#}P< 0.05$ vs CLP group.

3.3. Inhibiting Ferroptosis Decreased LCN2 Expression and Alleviate Myocardial Damage in Sepsis

Table 1 treatment, it showed the significant recovery in cardiac function (Figure 3 A-D, $P < 0.001$-0.01). In CLP group, HE staining also revealed that myocardial fibers were broken and inflammatory cell infiltration was increased (Figure 3 G), the levels of CK-MB and LDH were significantly decreased, with the increase of SOD level, suggesting that myocardial injury in CLP group was happened, DXZ and Fer-1 effectively reversed the myocardial injury (Figure 3 E, F, L, $P < 0.001$-0.01). The levels of serum IL-6 and TNF-α in CLP group were significantly higher than those in Sham group, DXZ and Fer-1 decreased the levels of IL-6 and TNF-α (Figure 3 M, N, $P < 0.001$-0.01). The biochemical characteristics of ferroptosis MDA and ROS levels [42] were higher in CLP mice compared to Sham mice (Figure 3 J, K, $P < 0.001$). The morphological changes of mitochondria was happened in CLP group [43] including mitochondrial shrinkage, increased membrane density, and mitochondrial cristae disruption (Figure 3 H). ELISA and western blot analysis both confirmed the elevated LCN2 expression level in cardiac tissue in CLP mice (Figure 2 C, E, $P < 0.001$-0.01), which were significantly reduced in DXZ+CLP and Fer-1+CLP groups. These results indicate that in SIMI, LCN2 expression is closely associated with ferroptosis. Inhibiting ferroptosis reduced LCN2 expression and mitigated SIMI.

 doi:10.20944/preprints202606.0308.v1

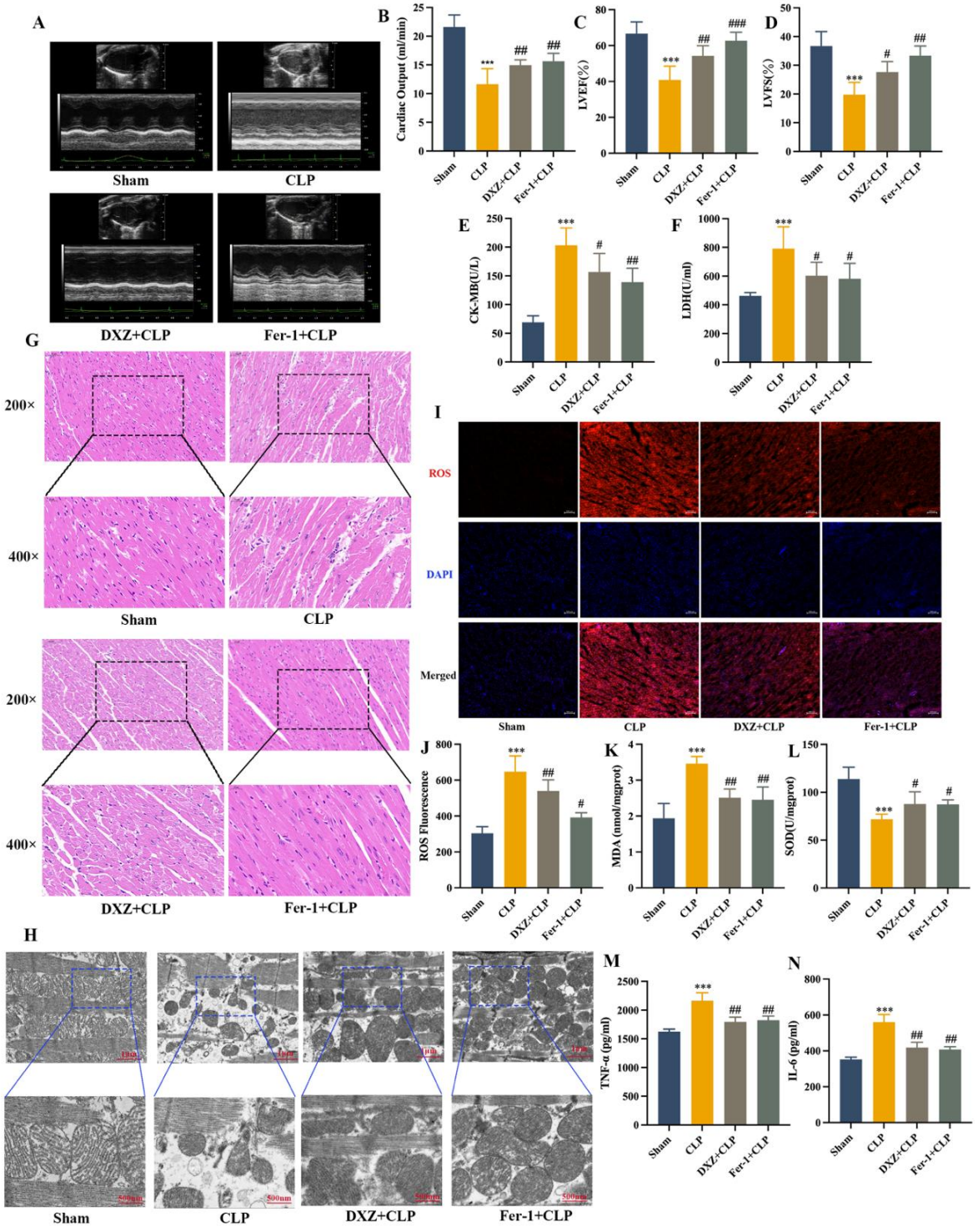

Figure 3. Inhibiting ferroptosis decreases LCN2 expression and alleviate myocardial damage in sepsis. A, G, H, I: Representative images of echocardiographic M-mode (A), H&E (G), transmission electron microscopy (H) and fluorescence probe for ROS in cardiac tissues (I) (Scale bar = 100 μm) in different groups. B-D: Echocardiographic parameters. cardiac output (B); left ventricle ejection fraction (C); left ventricular fractional shortening (D). E-F: The serum CK-MB (E) and LDH (F) levels in each group. Data are presented as mean ± SD (n=6). $^{***}P < 0.001$ vs Sham group, $^{###}P< 0.001$, $^{##}P< 0.01$, $^{#}P< 0.05$ vs CLP group.

3.4. Knockdown of LCN2 Improves Mitochondrial Function and Alleviates Sepsis-Induced Ferroptosis

To assess the protective role of inhibition LCN2 against SIMI, the wild-type C57BL/6 mice were injected intravenously with 2×10^{11}PFUs AAV9-ShLCN2 to knockdown LCN2 efficiency. qPCR and

 doi:10.20944/preprints202606.0308.v1

western blot results confirmed after the mice were injected with AAV9-ShLCN2, myocardial LCN2 at mRNA and protein expression levels were reduced (Fig 4 A-C, $P < 0.001$). Knockdown of LCN2 improved cardiac function parameters (Fig 4 K-N, $P < 0.001$-0.01), reduced myocardial fiber rupture, and inflammatory cell infiltration (Figure 4 A-C, $P < 0.001$). The ultrastructure results showed fewer mitochondrial morphological changes, MMP and mitochondrial function index - COX IV protein expression were increased, with the decrease of Cyto C protein expression, suggesting that mitochondrial damage was reduced after knockdown of LCN2 in CLP mice. Meanwhile, myocardial ROS level was decreased, the ferroptosis-related proteins Ferritin, FPN1, Mito GPX4 and Mito DHODH were increased ($P < 0.001$). Overall, LCN2 knockdown protects the myocardium against cyto- and mitochondrial ferroptosis in CLP mice.

3.5. DHODH as a Key Protein of Ferroptosis Against LCN2 Induced Myocardial Damage in Sepsis

LCN2, an innate immune protein, has emerged as a critical iron regulatory protein during physiological and inflammatory conditions [44]. Through molecular docking and immunoprecipitation experiment, we observed that LCN2 interacts strongly with DHODH protein (Figure 4O). DHODH, a rate-limiting enzyme for de novo pyrimidine nucleotide synthesis located in mitochondria, plays a crucial role in mitochondrial oxidative phosphorylation and respiratory chain [10]. For observing the relationship between LCN2 and mitochondrial ferroptosis, the mice were also treated with the specific DHODH inhibitor Brequinar (20 mg/kg, i.p), and mito-GPX4 inhibitor Fin56 (10 mg/kg, i.p) on knockdown-LCN2 mice before CLP surgery (Figure 4 G). the results showed compared with the AAV9-ShLCN2+CLP group, Brequinar and Fin56 exacerbated myocardial injury with increased LCN2 protein expression (Fig 5 G, $P < 0.001$), decreased MSS scores (Fig 4 H), ruptured myocardial fiber, increased red blood cells and inflammatory cell infiltration (Fig 4 O). Elevated serum levels of CK-MB, LDH, IL-6, TNF-α, increased MDA and ROS levels and decreased SOD level (Fig 4 I, G and Fig 5 B, C, D, $P < 0.001$-0.01). ELISA kits and Western blot analysis results showed, compared with the AAV9-ShLCN2+CLP group, Brequinar decreased myocardial DHODH expression and elevated LCN2 levels, while Fin56 treatment showed no statistically significant changes in LCN2 and DHODH expressions. Meanwhile, in the AAV9-ShLCN2+CLP+Brequinar and AAV9-ShLCN2+CLP+Fin56 groups, it exhibited mitochondrial atrophy, increased membrane density, ridge breakage, partial mitochondrial outer membrane rupture (Figure 4 P), the decrease of mitochondrial COX IV expression (Figure 4 R), and the increase of cytoplasmic Cyto C expression (Fig 4 U) were also observed. These findings indicated that inhibition of DHODH and mito-GPX4 could eliminate the protective effect of LCN2-knockdown on mitochondrial function and exacerbate SIMI, but mito-GPX4 has no effect on LCN2 and DHODH.

 doi:10.20944/preprints202606.0308.v1

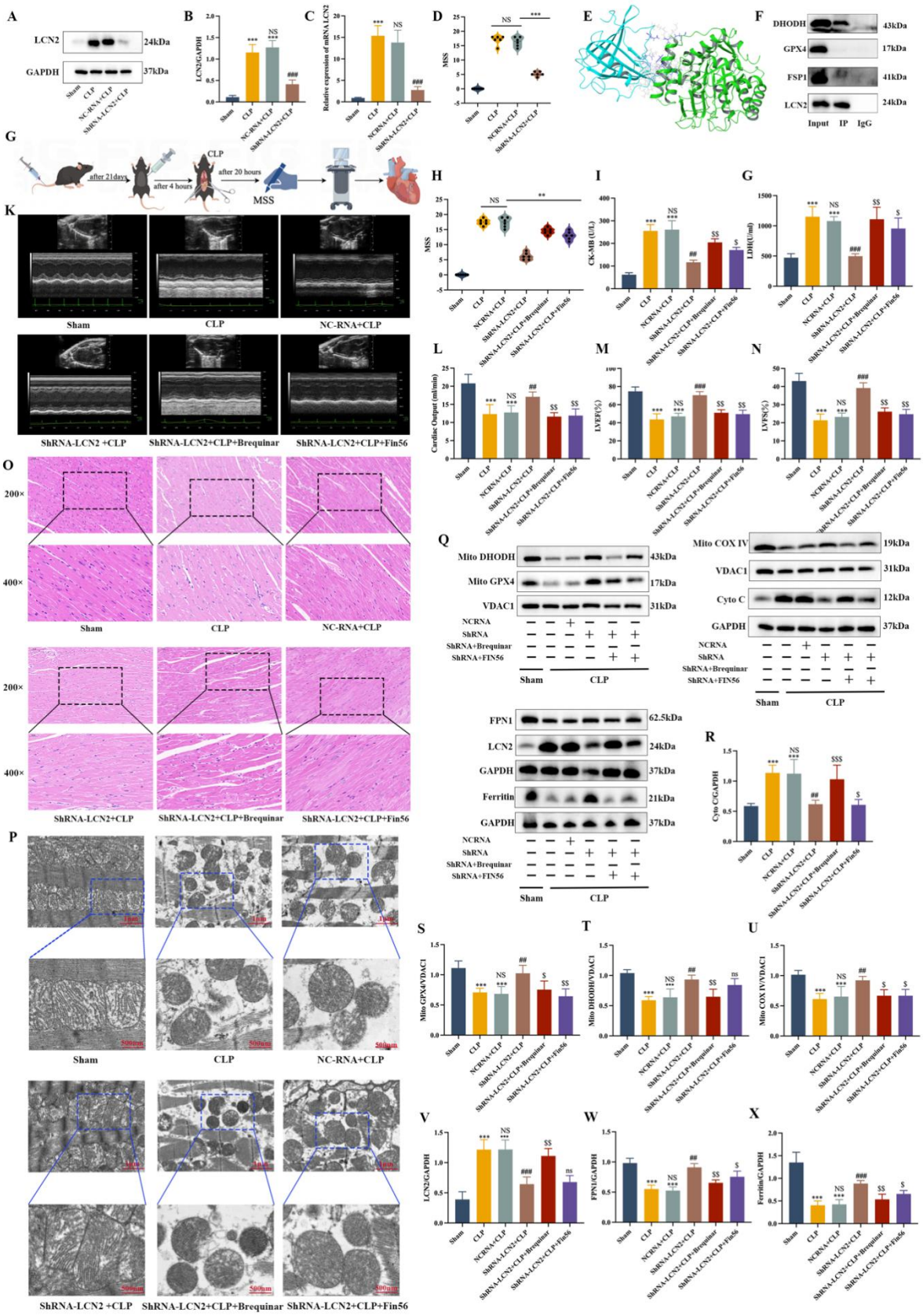

Figure 4. DHODH as a key protein of LCN2 affecting myocardial damage in sepsis. A, E, F, K, O, P: Representative images of Western blot results (A), molecular docking results (E, LCN2: green, DHODH: blue), immune-function precipitation results (F), echocardiographic M-mode (K), H&E (O) and transmission electron microscopy (P) in cardiac tissues in different groups. B: Changes in the protein expressions of LCN2 (n = 3). C: The LCN2 level at mRNA expression was detected in each group by q-PCR (n = 6). G: Experimental design

 doi:10.20944/preprints202606.0308.v1

drawing. D, H: Murine sepsis sorce. I-G: The serum CK-MB (I) and LDH (G) levels in each group. Echocardiographic parameters: cardiac output (L); left ventricle ejection fraction (M); left ventricular fractional shortening (N). Q: Representative images of the Western blot results. Changes in the protein expressions of Cyto C (R), Mito GPX4 (S), Mito DHODH (T), Mito COX IV (U), LCN2 (V), FPN1 (W) and Ferritin (X).Data are presented as mean ± SD (n=6). ***P< 0.001 vs Sham group, $^{###}$P < 0.001, $^{##}$P< 0.01 vs NC-RNA+CLP group, NS: P > 0.05 vs CLP group, $^{$$$}$P< 0.0o1, $^{$$}$P< 0.01, $^{$}$P< 0.05 vs ShRNA-LCN2+CLP group, ns P > 0.05 vs .ShRNA-LCN2+CLP group.

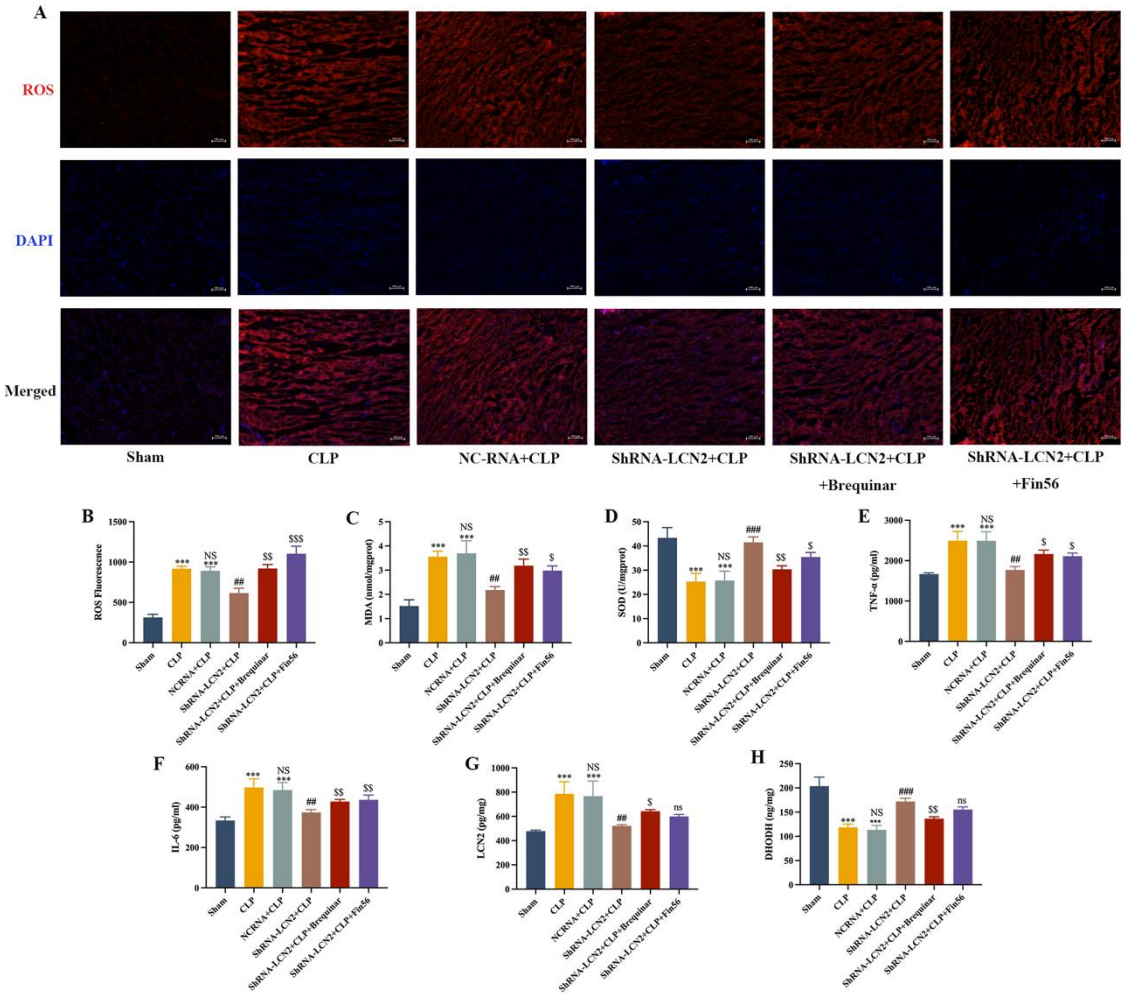

Figure 5. A: Representative images of fluorescence probe for ROS in cardiac tissues (Scale bar = 100 μm). B: The ROS fluorescence in each group. C-D: Changes of myocardial MDA (C) and SOD (D) levels in different groups. E-F: The serum TNF-α (E) and IL-6 (F) levels in each group. G-H: The cardiac LCN2 and DHODH levels in each group. Data are presented as mean ± SD (n=6). ***P< 0.001 vs Sham group, $^{###}$P < 0.001, $^{##}$P < 0.01 vs NC-RNA+CLP group, NS: P > 0.05 vs CLP group, $^{$$$}$P < 0.001, $^{$$}$P < 0.01, $^{$}$P < 0.05 vs ShRNA-LCN2+CLP group, ns P > 0.05 vs ShRNA-LCN2+CLP group.

3.6. Recombinant LCN2 Protein Induced Cardiomyocyte Injury and Triggers Ferroptosis

For further investigate the potential effect of LCN2 on ferroptosis, we used rLCN2 in HL-1 mouse cardiomyocytes. The results showed that addition of rLCN2 increased intracellular and mitochondrial ROS levels (Figure 6 B, D), elevated Fe^{2+} levels, decreased MMP (Figure 6 H), and reduced LCN2 (Figure 4 G, K) and ferroptosis-related proteins GPX4 and DHODH (Figure 6 J, F, L).

 doi:10.20944/preprints202606.0308.v1

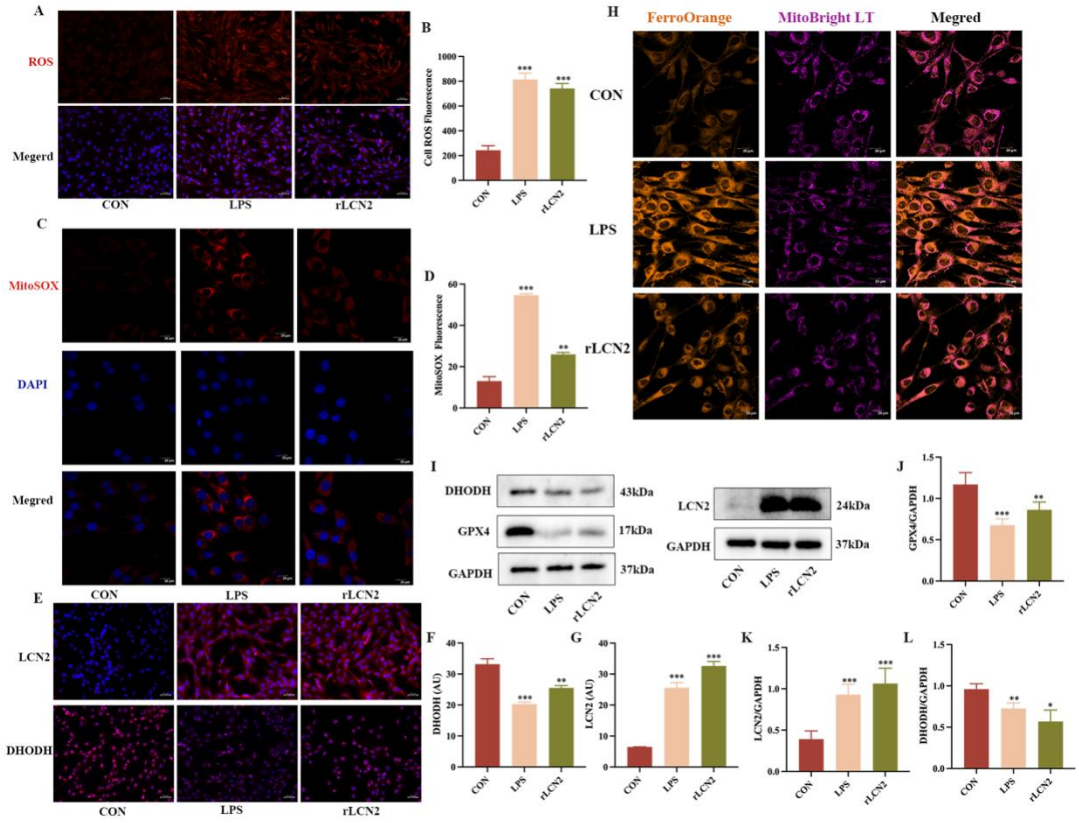

Figure 6. LCN2 induces ferroptosis in cardiomyocytes. A: Representative images of fluorescence probe for ROS in HL-1 cardiomyocytes (n=6, scale bar= 50 μm). B: The ROS fluorescence in each group. C: Images of mitochondrial ROS in different groups. D: Mitochondrial ROS fluorescence intensity analysis. (n=5, scale bar= 20 μm). E: Images of LCN2 and DHODH (red) and DAPI (blue) immunofluorescence staining. F, G: LCN2 and DHODH fluorescence intensity analysis. (n=6, scale bar= 50 μ m). H: Detection of intracellular $Fe^{2+}$and mitochondrial morphology of HL-1 cardiomyocytes in different groups (scale bar= 20 μm). I: Representative images of the Western blot results. Changes in the protein expressions of LCN2 (K), GPX4 (J) and DHODH (L) (n = 6). Data are presented as mean ± SD. $^{***}P < 0.001$, $^{**}P < 0.01$, $^{*}P < 0.05$ vs CON group.

3.7. Overexpression of DHODH Resists LPS-Induced Mouse Cardiomyocyte Injury

To determine whether DHODH is a key factor in LCN2 induced ferroptosis in sepsis, lentivirus overexpression of DHODH was performed in vitro, the transfection efficiency was verified by qPCR and Western blot (Fig 7 A-C, $P < 0.001$). The results showed ROS levels in cells and mitochondria were decreased in LPS-induced HL-1 cardiomyocyte model with DHODH-overexpression (Fig 7 A-C), lipid peroxidation levels and intracellular Fe^{2+} levels were decreased, and MMP was increased (Fig 7 H). GPX4, DHODH and FPN1 expressions were significantly increased, while LCN2 protein expression was significantly decreased (Fig 7 M, N, O, $P < 0.001$-0.01). Treatment with rLCN2 reversed the effect of DHODH-overexpression in LPS-induced HL-1 cells.

 doi:10.20944/preprints202606.0308.v1

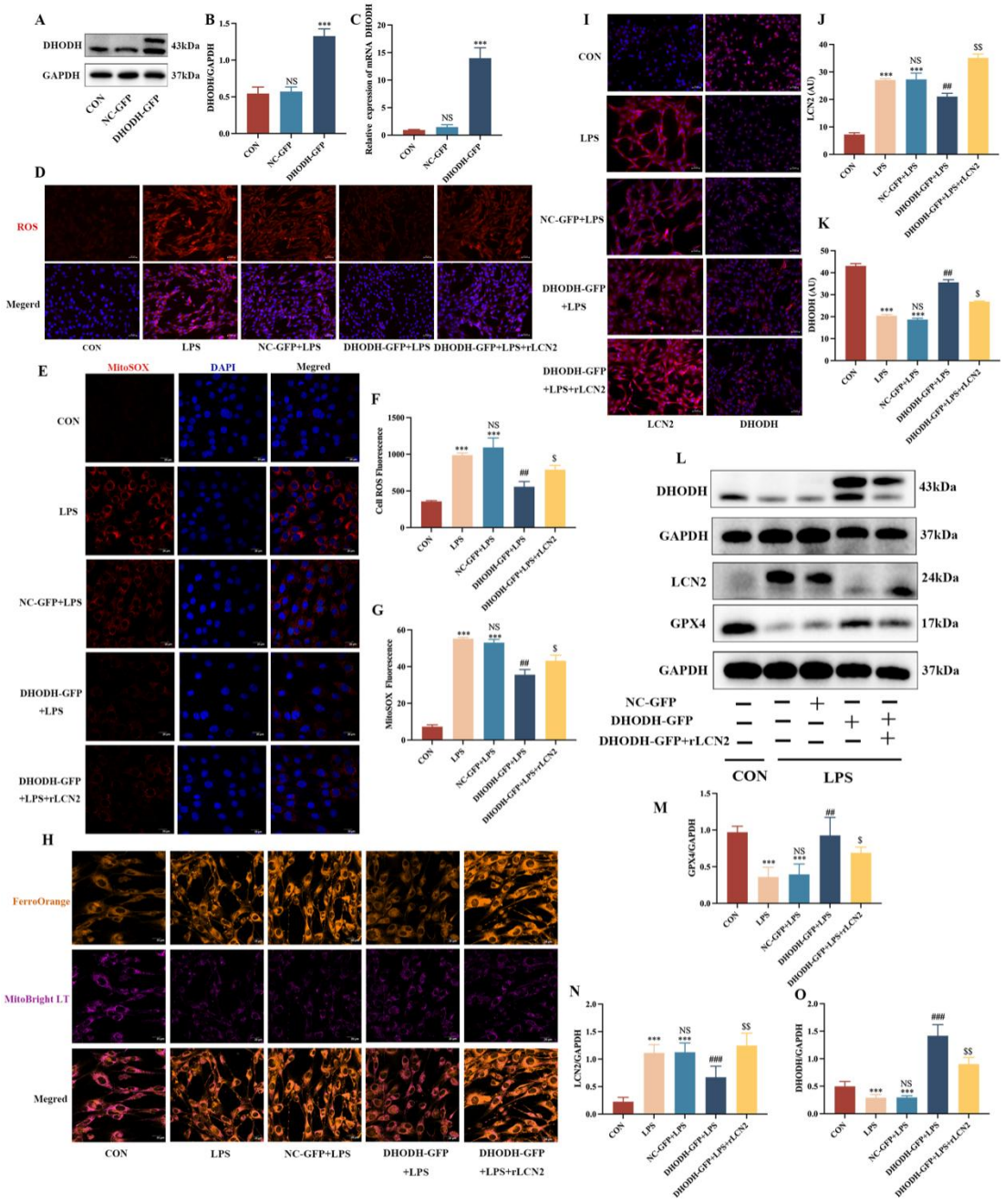

Figure 7. Overexpression of DHODH resists LPS-induced mouse cardiomyocyte injury. A: Representative images of Western blots. B: Changes in the protein expressions of DHODH (n=3). C: The LCN2 expression was detected by qPCR (n=6). D: Representative images of fluorescence probe for ROS in HL-1 cardiomyocytes (n=6, scale bar= 50 μm). F: The ROS fluorescence in each group. E: Images of mitochondrial ROS in different groups. G: Mitochondrial ROS fluorescence intensity analysis. (n=5, scale bar= 20 μm). I: Images of LCN2 and DHODH (red) and DAPI (blue) immunofluorescence staining. J, K: LCN2 and DHODH fluorescence intensity analysis. (n=6, scale bar= 50 μm). H: Detection of intracellular Fe^{2+} and mitochondrial morphology of HL-1 cardiomyocytes in different groups (scale bar= 20 μm). L: Representative images of the Western blot results. Changes in the protein expressions of GPX4 (M), LCN2 (N) and DHODH (O) (n = 6). Data are presented as mean ± SD. $^{***}P < 0.001$, $^{**}P < 0.01$, $^{*}P < 0.05$ vs CON group. NS: P>0.05 vs CON group (Fig8 B, C) , $^{\#\#}P< 0.01$ vs NC-GFP+LPS group, NS: P > 0.05 vs LPS group (Fig8 J, K, F, G, M, N, O), $^{\$\$\$}P< 0.001$, $^{\$\$}P< 0.01$, $^{\$}P< 0.05$ vs DHODH-GFP+LPS group.

3.8. LCN2 Activates Ferroptosis Through Inhibiting DHODH Expression via STAT3 Signaling

STAT3 signaling pathway plays a critical role in various biological processes, and LCN2 induces ferroptosis by activating STAT3 pathway [45]. STAT3 is closely associated with DHODH protein and

 doi:10.20944/preprints202606.0308.v1

mitochondrial function [46]. We sought to explore whether STAT3 is involved in the regulation of LCN2 in myocardial damage caused by sepsis. The results showed, stimulation of HL-1 cells with rLCN2 increased phosphorylation STAT3 (p-STAT3) (Figure 8 A-E). When compared with LPS-induced DHODH-overexpression HL-1 cells, rLCN2 reduced DHODH protein expression, while increased p-STAT3 expression (Figure 8 F-K). Knockdown of LCN2 reduced p-STAT3 expression level, which were reversed by DHODH-specific inhibitor Brequinar but not by GPX4 inhibitor Fin56 (Fig 8 L-N).

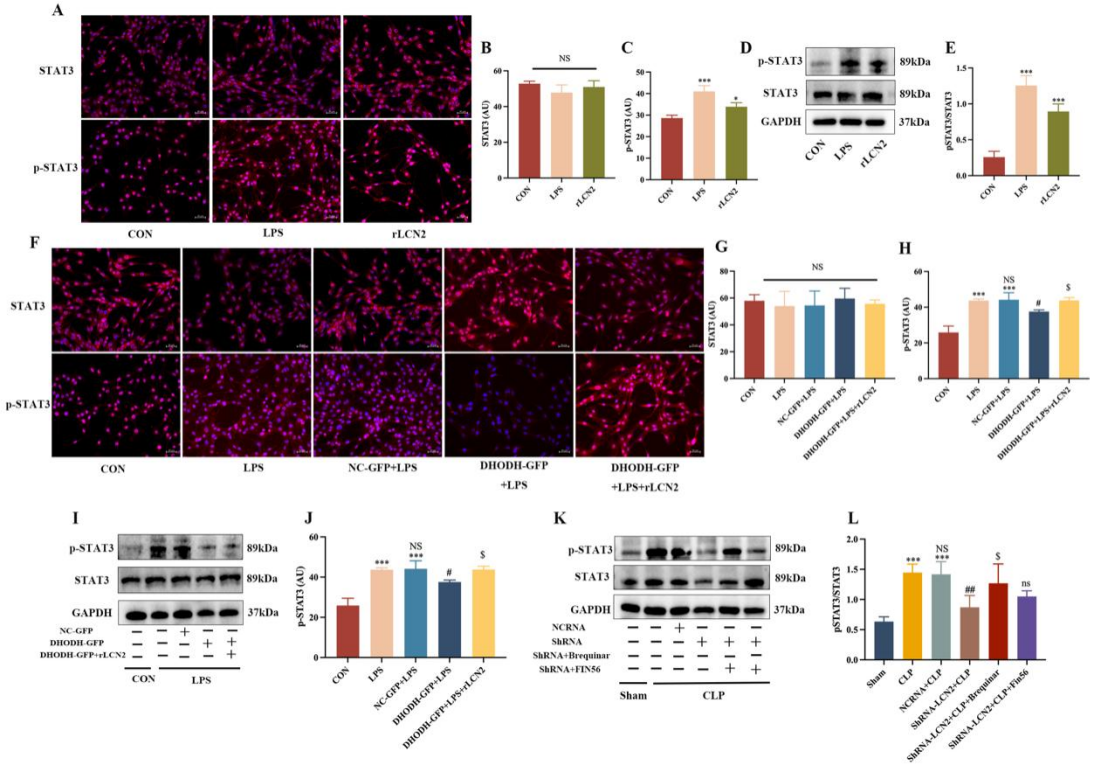

Figure 8. LCN2 activates ferroptosis by inhibiting DHODH expression via the STAT3 signaling. A, F: Images of STAT3 and p-STAT3 (red) and DAPI (blue) immunofluorescence staining. B, C, G, H: STAT3 (B, G) and p-STAT3 (C, H) fluorescence intensity analysis. (n=6, scale bar= 50 μm). D, I, L: Representative images of the Western blot results. Changes in the protein expressions of P-STAT3 (E, J, L). Data are presented as mean ± SD (n = 6). ***P < 0.001, **P < 0.01, *P < 0.05 vs CON group. NS: P>0.05 vs CON group (Figure 8 B, C) , $^{\#\#}$P< 0.01 vs NC-GFP+LPS group, NS: P > 0.05 vs LPS group (Fig8 H, J), $^{\$\$\$}$P< 0.001, $^{\$\$}$P< 0.01, $^{\$}$P< 0.05 vs DHODH-GFP+LPS group (Figure 8 B, C, E, G, H, J). ***P< 0.001 vs Sham group, $^{\#\#\#}$P < 0.001, $^{\#\#}$P< 0.01 vs NC-RNA+CLP group, NS: P > 0.05 vs CLP group, $^{\$\$\$}$P< 0.0o1, $^{\$\$}$P< 0.01, $^{\$}$P< 0.05 vs ShRNA-LCN2+CLP group, ns P > 0.05 vs ShRNA-LCN2+CLP group (Figure 8 L).

4. Discussion

Sepsis is a life-threatening systemic reactive disease, and myocardial dysfunction is a major cause of its high mortality rate [47]. Cardiomyocytes, as terminally differentiated cells, undergo irreversible deterioration of cardiac function once damaged by sepsis. The studies have indicated that cardiomyocyte death is a key factor in SIMI, thus alleviating cardiomyocyte death in sepsis is considered as an important therapeutic approach. Cell death can be categorized into apoptotic and non-apoptotic processes, including necrosis, pyroptosis, ferroptosis, et al [48]. Numerous studies have demonstrated that ferroptosis is involved in various pathological processes [49], and is closely linked to SIMI. Currently, it is believed that ferroptosis involves multiple metabolic pathways, cytosolic and mitochondrial GPX4 both play the major protective role against lipid peroxidation [50], while FSP1 acts primarily on the plasma membrane [51], and DHODH functions in mitochondria [52]. These different ferroptosis pathways interact each other, promoting myocardial injury and

 doi:10.20944/preprints202606.0308.v1

dysfunction. In this study, our results showed that inhibition of ferroptosis with Fer-1 and the iron chelator DXZ reduced myocardial LCN2 expression, alleviated oxidative stress and myocardial injury caused by ferroptosis from these different pathways. Therefore, intensively investigating the relationship of LCN2 and ferroptosis pathways is crucial for the prevention and treatment of SIMI.

LCN2 is an acute-phase protein that regulates various cellular processes, and plays a significant pathogenic role in acute and chronic inflammation, cancer, central nervous system diseases, and metabolic diseases [53]. It is currently used as a biomarker for renal injury [54], high plasma LCN2 levels predict high mortality and cardiac dysfunction in patients with severe sepsis and septic shock [55]. As a transporter regulating intracellular and extracellular iron levels, LCN2 directly controls iron metabolism [56], maintaining iron homeostasis is vital for cardiac function [57], and the increasing evidence suggests that LCN2 plays a critical role in maintaining cardiovascular iron homeostasis [58].

In our study, from the in vitro experiments, we determined that LCN2 could induce an increase in Fe^{2+} content, intracellular and mitochondrial ROS levels and inhibition of GPX4 in HL-1 mouse cardiomyocytes, leading to oxidative stress and ferroptosis. In vivo study, in the LCN2-knockdown mice, ferroptosis was reduced and SIMI was rescued. these results suggest that LCN2 is a key factor causing SIMI through activation of ferroptosis. We also found that exogenous LCN2 protein stimulation in HL-1 cells induced mitochondrial dysfunction and activated p-STAT3 expression, while myocardial p-STAT3 activation was inhibited in LCN2-knockdown mice. Thus, we conclude that LCN2 regulates ferroptosis in SIMI through activation of STAT3 signaling pathway.

To further investigate the correlation between LCN2 and ferroptosis, we performed molecular docking to analyze for macromolecule-macromolecule interactions, and found a favorable docking effect between LCN2 and DHODH. Immunoprecipitation experiments using LCN2 as bait pulled down GPX4, FSP1, and DHODH proteins. DHODH protein was detected in the precipitated complex, while GPX4 and FSP1 were not detected, suggesting that LCN2 may act directly through the mitochondrial DHODH-mediated ferroptosis pathway. DHODH, which locates in mitochondria, is an essential enzyme for de novo pyrimidine synthesis and a therapeutic target in several cancers [11–16]. Recent studies have indicated that inhibiting DHODH may suppress tumor growth by inducing ferroptosis [10]. However, the mechanism between DHODH and LCN2 remains unknown. In our study, in the knockdown-LCN2 septic mice, we observed the elevated DHODH expression, improved cardiac function, reduced lipid peroxidation, decreased inflammatory cell infiltration, and lower oxidative stress levels. Similarly, in LPS-induced HL-1 cardiomyocyte sepsis model, LCN2 expression was increased while DHODH expression was decreased. Addition of exogenous LCN2 recombinant protein to normal cardiomyocyte reduced DHODH expression and increased ROS and Fe^{2+} levels, indicating that LCN2 inhibited DHODH directly to induce ferroptosish. Inhibition of myocardial LCN2 expression increased DHODH expression, reduced ferroptosis, and provided the cardioprotective role.

In our study, we furtherly observed that the protective effects of knockdown-LCN2 were counteracted by DHODH inhibitor Brequinar, not by mitochondrial GPX4 inhibitor Fin56 in septic mice. As we know, DHODH is a crucial component of the mitochondrial respiratory chain and involved in energy metabolism and ATP production [59], we then assessed that mitochondrial function by measuring cyto C and COX IV protein expressions, and ROS production. In the LPS-induced DHODH-overexpression HL-1 cell model, the results showed that the decreased mitochondrial ROS levels, recovered MMP, improved mitochondrial morphological damage, at the same time, p-STAT3 protein expression level was decreased, while exogenous rLCN2 increased mitochondrial ROS levels, decreased MMP, and damaged mitochondrial morphology. The protective effect of DHODH-overexpression was reversed by exogenous rLCN2, and p-STAT3 protein expression level was increased. Similarly, Brequinar, the DHODH inhibitor, alleviated the protective role and elevated p-STAT3 level in LCN2 -knockdown septic mice, mitochondrial GPX4 inhibitor Fin56 had no effect on p-STAT3. The results further indicates that LCN2 aggravates mitochondrial ferroptosis in SIMI through increasing STAT3 phosphorylation to decrease DHODH.

 doi:10.20944/preprints202606.0308.v1

5. Conclusions

In sepsis induced myocardial injury, myocardial LCN2 promotes mitochondrial ferroptosis. Knockdown of LCN2 protected against SIMI through elevating DHODH and dephosphorylation of STAT3. Our study is the first time to demonstrate the interaction between myocardial LCN2 and DHODH in septic mice, it provides the new insight for preventing sepsis induced myocardial injury.

Author Contributions:. Lu Li: Writing – review & editing, Writing – original draft, Methodology, Software Data curation, Conceptualization. Yuping Li: Methodology, Visualization, Data curation. Yixuan Hao: Investigation, Data curation. Mengjie Yu: Visualization, Validation. Yuming Zhang: Resources, Investigation. Shicheng Xia: Visualization. Jiahui Wang: Methodology. Hongwei Ye: Writing – review & editing, Supervision, Methodology. Qin Gao: Writing – review & editing, Supervision, Resources, Funding acquisition, Conceptualization.

Funding: The present study was supported by Anhui Province Education Major Project (grant no. 2022AH040213), Anhui Province Project of Excellent Scientific Research and Innovation Team (grant no. 2022AH010083), Project of Bengbu Medical College Science and Technology Program (grant no. 2024byfy004), Open Project of Anhui Provincial Key Laboratory of Infection and Immunity (grant no. I&I-2024-K01), and Graduate Research Innovation Program of Bengbu Medical University (grant no. Byycx22014), China.

Institutional Review Board Statement: This study was approved by the Ethics Committee of Bengbu Medical College (Ethics number: [2023] No. 520), and all experiments complied with the "Regulations on the Administration of Laboratory Animals.

Informed Consent Statement: Not applicable.

Data Availability Statement: The original contributions presented in this study are included in the article/supplementary material. Further inquiries can be directed to the corresponding author.

Conflicts of Interest: The authors declare no conflict of interest.

References

1. Napolitano, L.M. Sepsis 2018: Definitions and Guideline Changes. *Surgical Infections* **2018**, *19*, 117–125. https://doi.org/10.1089/sur.2017.278.
2. Cookson, B.T.; Brennan, M.A. Pro-Inflammatory Programmed Cell Death. *Trends Microbiol* **2001**, *9*, 113–114. https://doi.org/10.1016/s0966-842x(00)01936-3.
3. Buerke, U.; Carter, J.M.; Schlitt, A.; Russ, M.; Schmidt, H.; Sibelius, U.; Grandel, U.; Grimminger, F.; Seeger, W.; Mueller-Werdan, U.; et al. Apoptosis Contributes to Septic Cardiomyopathy and Is Improved by Simvastatin Therapy. *Shock* **2008**, *29*, 497–503. https://doi.org/10.1097/shk.0b013e318142c434.
4. Mou, Y.; Wang, J.; Wu, J.; He, D.; Zhang, C.; Duan, C.; Li, B. Ferroptosis, a New Form of Cell Death: Opportunities and Challenges in Cancer. *J Hematol Oncol* **2019**, *12*. https://doi.org/10.1186/s13045-019-0720-y.
5. Gan, B. Mitochondrial Regulation of Ferroptosis. *J Cell Biol* **2021**, *220*, e202105043. https://doi.org/10.1083/jcb.202105043.
6. Fang, X.; Wang, H.; Han, D.; Xie, E.; Yang, X.; Wei, J.; Gu, S.; Gao, F.; Zhu, N.; Yin, X.; et al. Ferroptosis as a Target for Protection against Cardiomyopathy. *Proc Natl Acad Sci U S A* **2019**, *116*, 2672–2680. https://doi.org/10.1073/pnas.1821022116.
7. Wang, B.; Jin, Y.; Liu, J.; Liu, Q.; Shen, Y.; Zuo, S.; Yu, Y. EP1 Activation Inhibits Doxorubicin-Cardiomyocyte Ferroptosis via Nrf2. *Redox Biol* **2023**, *65*, 102825. https://doi.org/10.1016/j.redox.2023.102825.
8. Ahola, S.; Rivera Mejías, P.; Hermans, S.; Chandragiri, S.; Giavalisco, P.; Nolte, H.; Langer, T. OMA1-Mediated Integrated Stress Response Protects against Ferroptosis in Mitochondrial Cardiomyopathy. *Cell Metab* **2022**, *34*, 1875-1891.e7. https://doi.org/10.1016/j.cmet.2022.08.017.

 doi:10.20944/preprints202606.0308.v1

9. Liu, C.; Zou, Q.; Tang, H.; Liu, J.; Zhang, S.; Fan, C.; Zhang, J.; Liu, R.; Liu, Y.; Liu, R.; et al. Melanin Nanoparticles Alleviate Sepsis-Induced Myocardial Injury by Suppressing Ferroptosis and Inflammation. *Bioact Mater* **2023**, *24*, 313–321. https://doi.org/10.1016/j.bioactmat.2022.12.026.
10. Mao, C.; Liu, X.; Zhang, Y.; Lei, G.; Yan, Y.; Lee, H.; Koppula, P.; Wu, S.; Zhuang, L.; Fang, B.; et al. DHODH-Mediated Ferroptosis Defence Is a Targetable Vulnerability in Cancer. *Nature* **2021**, *593*, 586–590. https://doi.org/10.1038/s41586-021-03539-7.
11. Li, L.; Ng, S.R.; Colón, C.I.; Drapkin, B.J.; Hsu, P.P.; Li, Z.; Nabel, C.S.; Lewis, C.A.; Romero, R.; Mercer, K.L.; et al. Identification of DHODH as a Therapeutic Target in Small Cell Lung Cancer. *Sci Transl Med* **2019**, *11*, eaaw7852. https://doi.org/10.1126/scitranslmed.aaw7852.
12. Sykes, D.B.; Kfoury, Y.S.; Mercier, F.E.; Wawer, M.J.; Law, J.M.; Haynes, M.K.; Lewis, T.A.; Schajnovitz, A.; Jain, E.; Lee, D.; et al. Inhibition of Dihydroorotate Dehydrogenase Overcomes Differentiation Blockade in Acute Myeloid Leukemia. *Cell* **2016**, *167*, 171-186.e15. https://doi.org/10.1016/j.cell.2016.08.057.
13. White, R.M.; Cech, J.; Ratanasirintrawoot, S.; Lin, C.Y.; Rahl, P.B.; Burke, C.J.; Langdon, E.; Tomlinson, M.L.; Mosher, J.; Kaufman, C.; et al. DHODH Modulates Transcriptional Elongation in the Neural Crest and Melanoma. *Nature* **2011**, *471*, 518–522. https://doi.org/10.1038/nature09882.
14. Koundinya, M.; Sudhalter, J.; Courjaud, A.; Lionne, B.; Touyer, G.; Bonnet, L.; Menguy, I.; Schreiber, I.; Perrault, C.; Vougier, S.; et al. Dependence on the Pyrimidine Biosynthetic Enzyme DHODH Is a Synthetic Lethal Vulnerability in Mutant KRAS-Driven Cancers. *Cell Chem Biol* **2018**, *25*, 705-717.e11. https://doi.org/10.1016/j.chembiol.2018.03.005.
15. Sykes, D.B. The Emergence of Dihydroorotate Dehydrogenase (DHODH) as a Therapeutic Target in Acute Myeloid Leukemia. *Expert Opin Ther Targets* **2018**, *22*, 893–898. https://doi.org/10.1080/14728222.2018.1536748.
16. Echizenya, S.; Ishii, Y.; Kitazawa, S.; Tanaka, T.; Matsuda, S.; Watanabe, E.; Umekawa, M.; Terasaka, S.; Houkin, K.; Hatta, T.; et al. Discovery of a New Pyrimidine Synthesis Inhibitor Eradicating Glioblastoma-Initiating Cells. *Neuro Oncol* **2020**, *22*, 229–239. https://doi.org/10.1093/neuonc/noz170.
17. Moreno-Navarrete, J.M.; Manco, M.; Ibáñez, J.; García-Fuentes, E.; Ortega, F.; Gorostiaga, E.; Vendrell, J.; Izquierdo, M.; Martínez, C.; Nolfe, G.; et al. Metabolic Endotoxemia and Saturated Fat Contribute to Circulating NGAL Concentrations in Subjects with Insulin Resistance. *Int J Obes (Lond)* **2010**, *34*, 240–249. https://doi.org/10.1038/ijo.2009.242.
18. Furutani, M.; Arii, S.; Mizumoto, M.; Kato, M.; Imamura, M. Identification of a Neutrophil Gelatinase-Associated Lipocalin mRNA in Human Pancreatic Cancers Using a Modified Signal Sequence Trap Method. *Cancer Lett* **1998**, *122*, 209–214. https://doi.org/10.1016/s0304-3835(97)00391-1.
19. Karlsen JR, Borregaard N, Cowland JB. Induction of neutrophil gelatinase-associated lipocalin expression by co-stimulation with interleukin-17 and tumor necrosis factor-alpha is controlled by IkappaB-zeta but neither by C/EBP-beta nor C/EBP-delta. J Biol Chem. **2010**;285(19):14088-100. https://doi.org/10.1074/jbc.M109.017129.
20. Seth, P.; Porter, D.; Lahti-Domenici, J.; Geng, Y.; Richardson, A.; Polyak, K. Cellular and Molecular Targets of Estrogen in Normal Human Breast Tissue. *Cancer Res* **2002**, *62*, 4540–4544.
21. Vazquez, D.E.; Niño, D.F.; De Maio, A.; Cauvi, D.M. Sustained Expression of Lipocalin-2 during Polymicrobial Sepsis. *Innate Immun* **2015**, *21*, 477–489. https://doi.org/10.1177/1753425914548491.
22. Sung, H.K.; Chan, Y.K.; Han, M.; Jahng, J.W.S.; Song, E.; Danielson, E.; Berger, T.; Mak, T.W.; Sweeney, G. Lipocalin-2 (NGAL) Attenuates Autophagy to Exacerbate Cardiac Apoptosis Induced by Myocardial Ischemia. *J Cell Physiol* **2017**, *232*, 2125–2134. https://doi.org/10.1002/jcp.25672.
23. Hemdahl, A.-L.; Gabrielsen, A.; Zhu, C.; Eriksson, P.; Hedin, U.; Kastrup, J.; Thorén, P.; Hansson, G.K. Expression of Neutrophil Gelatinase-Associated Lipocalin in Atherosclerosis and Myocardial Infarction. *Arterioscler Thromb Vasc Biol* **2006**, *26*, 136–142. https://doi.org/10.1161/01.ATV.0000193567.88685.f4.
24. F, A.; Ht, M.; Hg, S.; Ea, W.; A, A.; P, O.; T, B.; Tw, M.; M, M.; R, M.; et al. Lipocalin-2 Regulates the Inflammatory Response during Ischemia and Reperfusion of the Transplanted Heart. *American journal of transplantation : Official journal of the American Society of Transplantation and the American Society of Transplant Surgeons* **2007**, *7*. https://doi.org/10.1111/j.1600-6143.2006.01723.x.

 doi:10.20944/preprints202606.0308.v1

25. Choi, K.M.; Lee, J.S.; Kim, E.J.; Baik, S.H.; Seo, H.S.; Choi, D.S.; Oh, D.J.; Park, C.G. Implication of Lipocalin-2 and Visfatin Levels in Patients with Coronary Heart Disease. *Eur J Endocrinol* **2008**, *158*, 203–207. https://doi.org/10.1530/EJE-07-0633.
26. Xiong, H.; Luo, T.; He, W.; Xi, D.; Lu, H.; Li, M.; Liu, J.; Guo, Z. Up-Regulation of miR-138 Inhibits Hypoxia-Induced Cardiomyocyte Apoptosis via down-Regulating Lipocalin-2 Expression. *Exp Biol Med (Maywood)* **2016**, *241*, 25–30. https://doi.org/10.1177/1535370215591831.
27. Berger, T.; Togawa, A.; Duncan, G.S.; Elia, A.J.; You-Ten, A.; Wakeham, A.; Fong, H.E.H.; Cheung, C.C.; Mak, T.W. Lipocalin 2-Deficient Mice Exhibit Increased Sensitivity to Escherichia Coli Infection but Not to Ischemia-Reperfusion Injury. *Proc Natl Acad Sci U S A* **2006**, *103*, 1834–1839. https://doi.org/10.1073/pnas.0510847103.
28. Liu, Z.; Reba, S.; Chen, W.-D.; Porwal, S.K.; Boom, W.H.; Petersen, R.B.; Rojas, R.; Viswanathan, R.; Devireddy, L. Regulation of Mammalian Siderophore 2,5-DHBA in the Innate Immune Response to Infection. *J Exp Med* **2014**, *211*, 1197–1213. https://doi.org/10.1084/jem.20132629.
29. Wang, H.; Wang, Z.; Gao, Y.; Wang, J.; Yuan, Y.; Zhang, C.; Zhang, X. STZ-Induced Diabetes Exacerbates Neurons Ferroptosis after Ischemic Stroke by Upregulating LCN2 in Neutrophils. *Exp Neurol* **2024**, 114797. https://doi.org/10.1016/j.expneurol.2024.114797.
30. Li, Y.; Li, L.; Zhang, Y.; Yun, Q.; Du, R.; Ye, H.; Li, Z.; Gao, Q. Lipocalin-2 Silencing Alleviates Sepsis-Induced Liver Injury through Inhibition of Ferroptosis. *Ann Hepatol* **2025**, *30*, 101756. https://doi.org/10.1016/j.aohep.2024.101756.
31. Huang, Y.; Li, L.; Li, Y.; Lu, N.; Qin, H.; Wang, R.; Li, W.; Cheng, Z.; Li, Z.; Kang, P.; et al. Knockdown of LncRNA Lcn2-204 Alleviates Sepsis-Induced Myocardial Injury by Regulation of Iron Overload and Ferroptosis. *J Mol Cell Cardiol* **2024**, S0022-2828(24)00079-8. https://doi.org/10.1016/j.yjmcc.2024.05.007.
32. Janus Kinase Inhibition Ameliorates Ischemic Stroke Injury and Neuroinflammation Through Reducing NLRP3 Inflammasome Activation via JAK2/STAT3 Pathway Inhibition - PubMed Available online: https://pubmed.ncbi.nlm.nih.gov/34367186/ (accessed on 12 March 2024).
33. Hou, Y.; Wang, K.; Wan, W.; Cheng, Y.; Pu, X.; Ye, X. Resveratrol Provides Neuroprotection by Regulating the JAK2/STAT3/PI3K/AKT/mTOR Pathway after Stroke in Rats. *Genes Dis* **2018**, *5*, 245–255. https://doi.org/10.1016/j.gendis.2018.06.001.
34. Zhu, M.; Peng, L.; Huo, S.; Peng, D.; Gou, J.; Shi, W.; Tao, J.; Jiang, T.; Jiang, Y.; Wang, Q.; et al. STAT3 Signaling Promotes Cardiac Injury by Upregulating NCOA4-Mediated Ferritinophagy and Ferroptosis in High-Fat-Diet Fed Mice. *Free Radic Biol Med* **2023**, *201*, 111–125. https://doi.org/10.1016/j.freeradbiomed.2023.03.003.
35. Shiratori-Hayashi, M.; Koga, K.; Tozaki-Saitoh, H.; Kohro, Y.; Toyonaga, H.; Yamaguchi, C.; Hasegawa, A.; Nakahara, T.; Hachisuka, J.; Akira, S.; et al. STAT3-Dependent Reactive Astrogliosis in the Spinal Dorsal Horn Underlies Chronic Itch. *Nat Med* **2015**, *21*, 927–931. https://doi.org/10.1038/nm.3912.
36. Jiang, C.; Hou, M.; Sun, S.; Chen, G.; Bai, F.; Wang, S. Targeting Lcn2 to Inhibit Myocardial Cell Ferroptosis Is a Potential Therapy for Alleviating Septic Cardiomyopathy. *Inflammation* **2025**, *48*, 3066–3076. https://doi.org/10.1007/s10753-025-02250-3.
37. Rittirsch, D.; Huber-Lang, M.S.; Flierl, M.A.; Ward, P.A. Immunodesign of Experimental Sepsis by Cecal Ligation and Puncture. *Nat Protoc* **2009**, *4*, 31–36. https://doi.org/10.1038/nprot.2008.214.
38. Shrum, B.; Anantha, R.V.; Xu, S.X.; Donnelly, M.; Haeryfar, S.M.; McCormick, J.K.; Mele, T. A Robust Scoring System to Evaluate Sepsis Severity in an Animal Model. *BMC Res Notes* **2014**, *7*, 233. https://doi.org/10.1186/1756-0500-7-233.
39. Qin Y, Shi Y, Yu Q, Yang S, Wang Y, Dai X, Li G, Cheng Z. Vitamin B12 alleviates myocardial ischemia/reperfusion injury via the SIRT3/AMPK signaling pathway. Biomed Pharmacother. **2023**;163:114761. https://doi.org/10.1016/j.biopha.2023.114761.
40. Wang, Z.; Liu, M.; Ye, D.; Ye, J.; Wang, M.; Liu, J.; Xu, Y.; Zhang, J.; Zhao, M.; Feng, Y.; et al. Il12a Deletion Aggravates Sepsis-Induced Cardiac Dysfunction by Regulating Macrophage Polarization. *Front Pharmacol* **2021**, *12*, 632912. https://doi.org/10.3389/fphar.2021.632912.

 doi:10.20944/preprints202606.0308.v1

41. Wang, D.; Li, X.; Jiao, D.; Cai, Y.; Qian, L.; Shen, Y.; Lu, Y.; Zhou, Y.; Fu, B.; Sun, R.; et al. LCN2 Secreted by Tissue-Infiltrating Neutrophils Induces the Ferroptosis and Wasting of Adipose and Muscle Tissues in Lung Cancer Cachexia. *J Hematol Oncol* **2023**, *16*, 30. https://doi.org/10.1186/s13045-023-01429-1.
42. Tang D, Chen X, Kang R, Kroemer G. Ferroptosis: Molecular mechanisms and health implications. Cell Res. **2021**;31(2):107-125. https://doi.org/10.1038/s41422-020-00441-1.
43. Hirschhorn, T.; Stockwell, B.R. The Development of the Concept of Ferroptosis. *Free radical biology & medicine* **2019**, *133*, 130. https://doi.org/10.1016/j.freeradbiomed.2018.09.043.
44. Xiao, X.; Yeoh, B.S.; Vijay-Kumar, M. Lipocalin 2: An Emerging Player in Iron Homeostasis and Inflammation. *Annu. Rev. Nutr.* **2017**, *37*, 103–130. https://doi.org/10.1146/annurev-nutr-071816-064559.
45. Wang, X.; Li, X.; Zuo, X.; Liang, Z.; Ding, T.; Li, K.; Ma, Y.; Li, P.; Zhu, Z.; Ju, C.; et al. Photobiomodulation Inhibits the Activation of Neurotoxic Microglia and Astrocytes by Inhibiting Lcn2/JAK2-STAT3 Crosstalk after Spinal Cord Injury in Male Rats. *J Neuroinflammation* **2021**, *18*, 256. https://doi.org/10.1186/s12974-021-02312-x.
46. Hosseini, M.; Dousset, L.; Michon, P.; Mahfouf, W.; Muzotte, E.; Bergeron, V.; Bortolotto, D.; Rossignol, R.; Moisan, F.; Taieb, A.; et al. UVB-Induced DHODH Upregulation, Which Is Driven by STAT3, Is a Promising Target for Chemoprevention and Combination Therapy of Photocarcinogenesis. *Oncogenesis* **2019**, *8*, 52. https://doi.org/10.1038/s41389-019-0161-z.
47. Evans, L.; Rhodes, A.; Alhazzani, W.; Antonelli, M.; Coopersmith, C.M.; French, C.; Machado, F.R.; Mcintyre, L.; Ostermann, M.; Prescott, H.C.; et al. Surviving Sepsis Campaign: International Guidelines for Management of Sepsis and Septic Shock 2021. *Intensive Care Med* **2021**, *47*, 1181–1247. https://doi.org/10.1007/s00134-021-06506-y.
48. Galluzzi, L.; Vitale, I.; Aaronson, S.A.; Abrams, J.M.; Adam, D.; Agostinis, P.; Alnemri, E.S.; Altucci, L.; Amelio, I.; Andrews, D.W.; et al. Molecular Mechanisms of Cell Death: Recommendations of the Nomenclature Committee on Cell Death 2018. *Cell Death Differ* **2018**, *25*, 486–541. https://doi.org/10.1038/s41418-017-0012-4.
49. Gao, M.; Monian, P.; Quadri, N.; Ramasamy, R.; Jiang, X. Glutaminolysis and Transferrin Regulate Ferroptosis. *Mol Cell* **2015**, *59*, 298–308. https://doi.org/10.1016/j.molcel.2015.06.011.
50. Feng, Y.; Madungwe, N.B.; Imam Aliagan, A.D.; Tombo, N.; Bopassa, J.C. Ferroptosis Inhibitor, Liproxstatin-1, Protects the Myocardium against Ischemia/Reperfusion Injury by Decreasing VDAC1 Levels and Rescuing GPX4 Levels. *Biochem Biophys Res Commun* **2019**, *520*, 606–611. https://doi.org/10.1016/j.bbrc.2019.10.006.
51. Bersuker, K.; Hendricks, J.; Li, Z.; Magtanong, L.; Ford, B.; Tang, P.H.; Roberts, M.A.; Tong, B.; Maimone, T.J.; Zoncu, R.; et al. The CoQ Oxidoreductase FSP1 Acts in Parallel to GPX4 to Inhibit Ferroptosis. *Nature* **2019**, *575*, 688–692. https://doi.org/10.1038/s41586-019-1705-2.
52. Mao, C.; Liu, X.; Zhang, Y.; Lei, G.; Yan, Y.; Lee, H.; Koppula, P.; Wu, S.; Zhuang, L.; Fang, B.; et al. DHODH-Mediated Ferroptosis Defence Is a Targetable Vulnerability in Cancer. *Nature* **2021**, *593*, 586–590. https://doi.org/10.1038/s41586-021-03539-7.
53. Ghosh, S.; Stepicheva, N.; Yazdankhah, M.; Shang, P.; Watson, A.M.; Hose, S.; Liu, H.; Weiss, J.; Zigler, J.S.; Valapala, M.; et al. The Role of Lipocalin-2 in Age-Related Macular Degeneration (AMD). *Cell Mol Life Sci* **2020**, *77*, 835–851. https://doi.org/10.1007/s00018-019-03423-8.
54. Kim, H.; Hur, M.; Lee, S.; Marino, R.; Magrini, L.; Cardelli, P.; Struck, J.; Bergmann, A.; Hartmann, O.; Di Somma, S.; et al. Proenkephalin, Neutrophil Gelatinase-Associated Lipocalin, and Estimated Glomerular Filtration Rates in Patients With Sepsis. *Ann Lab Med* **2017**, *37*, 388–397. https://doi.org/10.3343/alm.2017.37.5.388.
55. Wang, B.; Chen, G.; Li, J.; Zeng, Y.; Wu, Y.; Yan, X. Neutrophil Gelatinase-Associated Lipocalin Predicts Myocardial Dysfunction and Mortality in Severe Sepsis and Septic Shock. *Int J Cardiol* **2017**, *227*, 589–594. https://doi.org/10.1016/j.ijcard.2016.10.096.
56. Liu Z, Reba S, Chen WD, Porwal SK, Boom WH, Petersen RB, Rojas R, Viswanathan R, Devireddy L. Regulation of mammalian siderophore 2,5-DHBA in the innate immune response to infection. J Exp Med. **2014** ;211(6):1197-213. https://doi.org/10.1084/jem.20132629.

 doi:10.20944/preprints202606.0308.v1

57. Fang, X.; Cai, Z.; Wang, H.; Han, D.; Cheng, Q.; Zhang, P.; Gao, F.; Yu, Y.; Song, Z.; Wu, Q.; et al. Loss of Cardiac Ferritin H Facilitates Cardiomyopathy via Slc7a11-Mediated Ferroptosis. *Circulation Research* **2020**, *127*, 486–501. https://doi.org/10.1161/CIRCRESAHA.120.316509.
58. Huang, Y.; Zhang, N.; Xie, C.; You, Y.; Guo, L.; Ye, F.; Xie, X.; Wang, J. Lipocalin-2 in Neutrophils Induces Ferroptosis in Septic Cardiac Dysfunction via Increasing Labile Iron Pool of Cardiomyocytes. *Front Cardiovasc Med* **2022**, *9*, 922534. https://doi.org/10.3389/fcvm.2022.922534.
59. Martínez-Reyes I, Cardona LR, Kong H, Vasan K, McElroy GS, Werner M, Kihshen H, Reczek CR, Weinberg SE, Gao P, Steinert EM, Piseaux R, Budinger GRS, Chandel NS. Mitochondrial ubiquinol oxidation is necessary for tumour growth. Nature. **2020;**585(7824):288-292. https://doi.org/10.1038/s41586-020-2475-6.